Beyond Band Alignment: Hole Localization Driven Formation of Three Spatially Separated Long-Lived Exciton States in CdSe/CdS Nanorods

Kaifeng Wu, William E. Rodríguez-Córdoba, Zheng Liu, Haiming Zhu, and Tianquan Lian*

Department of Chemistry, Emory University, 1515 Dickey Drive, NE, Atlanta, Georgia 30322, United States

ABSTRACT Colloidal one-dimensional semiconductor nanoheterostructures have emerged as an important family of functional materials for solar energy conversion, although the nature of the long-lived exciton state and their formation and dissociation dynamics remain poorly understood. In this paper we study these dynamics in CdSe/CdS dot-in-rod (DIR) NRs, a representative of 1D heterostructures, and DIR-electron-acceptor complexes by transient absorption spectroscopy. Because of a quasi-type II band alignment of CdSe and CdS, it is often assumed that there exists one long-lived exciton state with holes localized in the CdSe seed and electrons delocalized among CdSe and CdS. We show that excitation into the CdS rod forms three distinct types of long-lived excitons that are spatially localized in the CdS rod, in and near the CdSe seed and in the CdS shell surrounding the seed. The branching ratio of forming these exciton states is controlled by the competition between the band offset driven hole localization to the CdSe seed and hole trapping to the CdS surface. Because of dielectric contrast induced strong electron–hole interaction in 1D materials, the competing hole localization pathways lead to spatially separated long-lived excitons. Their distinct spatial locations affect their dissociation rates in the presence of electron acceptors, which has important implications for the application of 1D heterostructures as light-harvesting materials.

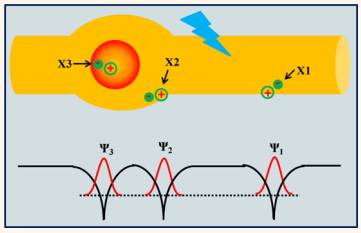

KEYWORDS: nanoheterostructure · CdSe/CdS · dot-in-rod · exciton localization · hole trapping · exciton dissociation

Recent advances in the synthesis of colloidal semiconductor heterostructures consisting of two or more material components have tremendously enriched the toolbox of semiconductor nanocrystals and produced new nanostructures with properties that cannot be achieved in single-component materials.[1−8] The alignment of the conduction band (CB) and valence band (VB) positions of the components in the heterostructure can be type I, in which the CB and VB of one material are nested between those of the other,[3,4] type II, when they are staggered with respect to each other,[9,10] or quasi-type II, when either the CB or VB band edge positions are similar in these materials. The band alignment in core/shell quantum dots (QDs) has been shown to dictate the distribution of electrons and holes in excitonic states, which has profound effects on their properties. For example, in type I core/shell QDs such as CdSe/ZnS, both the electron and hole wave functions are localized in the core in the lowest energy exciton state, which reduces the effect of surface defects and improves their emission properties.[11−16] On the other hand, the spatial separation of electrons and holes in type II heterostructures can lengthen the lifetime of single and multiple exciton states and improve their charge separation properties for light-harvesting applications.[10,17−19] In addition to material composition, the properties of nanoheterostructures can be further controlled by shape and size, as demonstrated in various one-dimensional (1D) colloidal nanorods (NRs).[7,20−27] Compared with QDs, these nanorods have larger absorption cross sections,[28−30] enhanced stabilities,[31,32] longer multiexciton lifetimes,[33−36] and linearly polarized emission[20,24,37−40] while retaining a size-tunable quantum confinement effect in the radial direction,[41,42] making them promising materials for light emitting,[43,44] optical gain,[34,45,46] or solar energy conversion applications.[47−54]

Among one-dimensional heterostructures, CdSe/CdS dot-in-rod (DIR) NRs have attracted the most intense research interest.[20,23,24,47,55−78]

* Address correspondence to tlian@emory.edu.

Received for review May 22, 2013 and accepted July 7, 2013.

Published online July 08, 2013
10.1021/nn402597p

They have been shown to enhance the charge separation efficiency in solar-to-fuel conversion systems compared to CdS nanorods or CdSe/CdS core/shell QDs.[47−49] The VB and CB offsets between bulk wurtzite CdSe and CdS are *ca.* +0.5 V and −0.3 to − 0 V, respectively, forming either a type I or quasi-type II heterojunction.[20,62] Despite recent investigations of this system by various techniques, including scanning tunneling spectroscopy,[62] transient absorption spectroscopy,[59,67] multiexciton emission,[65] time-resolved fluorescence decay,[73,74] and first-principles calculations,[63] the exact nature of the long-lived exciton states in the CdSe/CdS DIR structures remains a hotly debated topic. The band alignment in these materials has been reported to be type I,[62] quasi-type II,[59,74] or tunable from type I to quasi-type II depending on the core size and rod diameter,[65,73,75] as well as interfacial strain.[63] More recently, it has been suggested that even in quasi-type II DIRs the CB electron is likely localized near the CdSe core,[75,79,80] because of the strong electron−hole Coulomb attraction in one-dimensional structures.[81] Because the Bohr exciton radii of these materials (~5.4 nm in CdSe[82,83] and ~2.8 nm in CdS[84−86]) are relatively small compared to the rod length (typically 10's to 100's of nm), the fate of the initially generated electron−hole pairs depends on not only the band alignment but also their transport mechanism along the rod. The latter can be affected by deep hole traps on CdS NRs[87,88] and charge-transfer barrier at the CdSe/CdS interface.[66,89,90] Indeed, a recent study on CdSe/CdS tetrapods has demonstrated that the hole capturing efficiency by the CdSe core is not unity and there exist deep hole localized excitons on the CdS arms.[69]

In this paper, we report a study of exciton relaxation and dissociation dynamics in CdSe/CdS DIRs by transient absorption (TA) spectroscopy. By comparing TA spectra of DIR and DIR-electron-acceptor complexes, we show unambiguously that the bleaches of exciton bands in DIRs are caused by state-filling of the CB electron levels, similar to those observed in CdX (X = Te, Se, S) single-component or core/shell QDs. We show that in the lowest energy band edge exciton state the hole is confined in the CdSe core and the electron is delocalized among CdSe and CdS, consistent with a quasi-type II band alignment, although the electron wave function in the CdS shell is localized to regions near the CdSe core. Upon excitation of the CdS rod at 400 nm, three distinct long-lived exciton states are observed; only 46% of excitons can relax to the lowest energy band edge exciton state. Trapping of holes at the CdS rod or the CdS shell near the seed localizes excitons in those regions. Due to their distinct spatial locations, these excitons have different dissociation rates in the presence of electron acceptors. Our study suggests that in 1D heterostructures, such as CdSe/CdS DIR, the fate of the exciton is determined not only by the band offset but also by exciton trapping and localization processes that sensitively depend on the microscopic electronic and morphological heterogeneity of the materials.

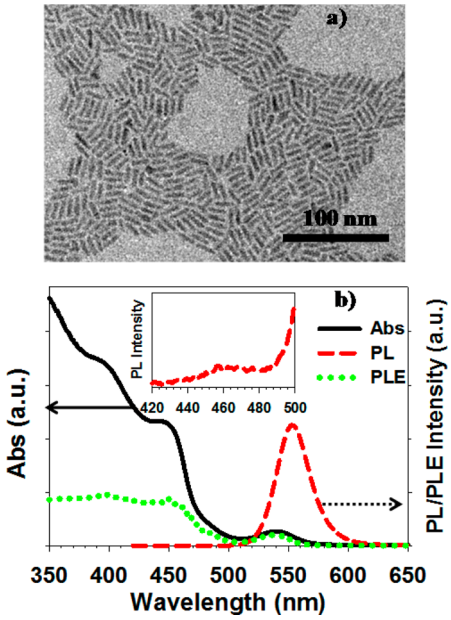

Figure 1. (a) Representative transmission electron microscopy image of CdSe/CdS DIRs. (b) UV−visible absorption spectrum (black solid line), photoluminescence (PL) spectrum measured with 400 nm excitation (red dashed line), and photoluminescence excitation (PLE) spectrum measured at 553 nm (green dashed line) of CdSe/CdS DIRs dispersed in chloroform. In the PLE spectrum, we have scaled the emission intensity to match the absorbance at 540 nm for better comparison. Inset: Enlarged view of the PL spectrum between 420 and 500 nm.

RESULTS AND DISCUSSIONS

Static Absorption and Emission Spectra. A representative TEM image of CdSe/CdS DIRs used for this study is shown in Figure 1a. The histograms of length (Figure S1a) and diameter (Figure S1b) distributions show an average length of 16.5 (±1.1) nm and diameter of 3.5 (±0.3) nm, respectively. Some of the rods show a bulb-like region with slightly large diameter near one end of the rod (Figure S1c), similar to previous reports.[23,66] The bulb region is believed to indicate the location of the seed from which asymmetric growth along the rod (*vs* the radial direction) occurs in the growth progress.[66] Due to the presence of these bulb structures, the diameter statistics is done at the centers of the DIRs.

The static absorption and emission spectra of DIRs are displayed in Figure 1b. The lowest absorption peak at ~540 nm can be assigned to the first excitonic transition, labeled as B3 in Scheme 1b, from the valence band edge in the CdSe core to the lowest energy conduction level of the DIR, because it is close to the band edge emission peak position (Figure 1b). It is below the onset of CdS absorption and red-shifted by about 0.18 eV with respect to the 1S exciton band of

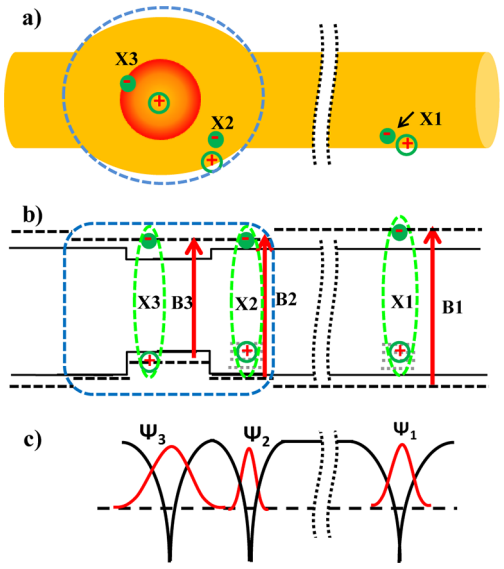

Scheme 1. (a) Schematic structure of a CdSe/CdS DIR prepared by seeded growth, showing a CdSe seed surrounded by a CdS rod and bulb-like region near the seed (blue dashed line). Also shown are the locations of three types of excitons (X1, X2, and X3). (b) Schematic energy level diagram for CdSe/CdS DIR, showing bulk band edges of CdS and CdSe (black solid lines), lowest electron and hole energy levels in CdSe core, CdS bulb, and CdS rod (black dashed lines), and sub-band-gap hole trap states in CdS (gray dotted lines). Also shown are the electron and hole levels of the X1, X2, and X3 excitons (green dashed curves) and the three (B1, B2, B3) lowest energy optically allowed exciton absorption bands in the static absorption spectra (red arrows). (c) Schematic electron wave functions of X1, X2, and X3 confined in the 1D Coulomb potential.

the starting CdSe seed. The red-shift indicates the extension of the electron wave function into the CdS shell/rod, which is indicative of a quasi-type II band alignment between CdSe and CdS and will be further discussed below. The peaks at ~400 and 450 nm can be attributed to the 1Π and 1Σ (labeled as B1 in Scheme 1b) 1D excitonic transitions, respectively, of the CdS rod in the DIR,[88] because of their resemblance to transitions in CdS NRs.[7,23,24,87,88,91] The contribution of CdSe core based transitions in this spectral region is negligible due to the much larger volume of the CdS rod.[59] In addition to these pronounced features, there exists an absorption feature near 480 nm (labeled as B2 in Scheme 1b), which can be attributed to the lowest energy transition of the CdS in the bulb region surrounding the CdSe seed.[66] Because of the larger diameter in the bulb compared to the rod region, the carrier confinement energy is lower, which accounts for the lower transition energy. A similar CdS-based absorption band has been seen in CdSe/CdS core/shell QDs of similar sizes.[92−96] In Figure S2, we show that the absorption spectrum below 2.8 eV (440 nm) can be fit by the sum of three Gaussian peaks with centers at 2.76 eV (449 nm), 2.58 eV (480 nm), and 2.30 eV (539 nm), corresponding to B1, B2, and B3 transitions, respectively. This assignment will be supported by transient absorption study of these DIRs to be discussed below.

The photoluminescence (PL) of DIRs after 400 nm excitation has a peak at 553 nm, corresponding to the emission from the band edge excitonic state (X3) of the DIR.[20] An expanded view of the PL spectrum from 420 to 500 nm (inset in Figure 1b) reveals a weak yet discernible peak at ~460 nm, which can be assigned to band edge emission of CdS NRs.[88] This suggests that not all excitons generated with 400 nm excitation relax down to the band edge exciton state prior to their radiative recombination. In addition to the band edge emission, CdS rod based emission can also contain a broad trap state emission band between 500 and 900 nm,[88] which may be too weak to be observed in CdSe/CdS DIRs due to its overlap with the much more intense X3 exciton emission band at 553 nm.

To further investigate the fate of excitons in DIR, we have also measured photoluminescence excitation (PLE) spectra, in which the PL intensity at 553 nm as a function of the excitation wavelength was recorded (Figure 1b). Accounting for the wavelength-dependent absorbance, the relative emission quantum yields (QYs) at 400, 480, and 540 nm excitations are estimated to be 0.46, 0.84, and 1, respectively. The absolute QYs at 400 nm excitation (using coumarin 343 as reference[97]) and at 540 nm excitation (using rodamine 6G as reference[98]) were also determined independently to be 22.5(±1.2)% and 48.7(±2.0)%, respectively. The ratio between the QYs at these two wavelengths (0.46) agrees well with the relative QY estimated from the PLE spectrum. The smaller QY at 400 nm excitation suggests that 54% of the excitons generated at the CdS rod do not reach the band edge (X3) exciton state. This is consistent with the observation of the CdS rod based emission at 460 nm discussed above.

Nature of Lowest Energy Band Edge Exciton (X3) State. The TA spectra of DIRs (from 0.1 ps to 50 ns) after 540 nm excitation are shown in Figure 2a. The TA spectra measured with 480 and 400 nm excitation will be discussed later. The excitation pulse energies (and the corresponding estimated numbers of excitons per DIR) were 13 nJ (0.008), 7.5 nJ (0.007), and 5.0 nJ (0.02) at 540, 480, and 400 nm, respectively. The details for estimating the number of excitons are provided in the Supporting Information. At these low excitation conditions, contributions of multiexciton dynamics to the observed TA signature can be neglected. There are two main bleach features at 540 and 480 nm. Compared with the static absorption spectrum in Figure 1b, we can assign the feature at 540 nm to photoinduced bleach of the B3 exciton band (or B3 bleach) and the feature at 480 nm to the bleach of the B2 band. This feature cannot be assigned to high-energy transition of CdSe seed. This is supported by a comparison with the TA spectrum of a bare CdSe core-only QD with similar confinement energy (Figure S3 in the Supporting Information), which shows derivative-like features in this wavelength range (430−480 nm) due to the Stark effect of 1S excitons on higher energy transitions.[99]

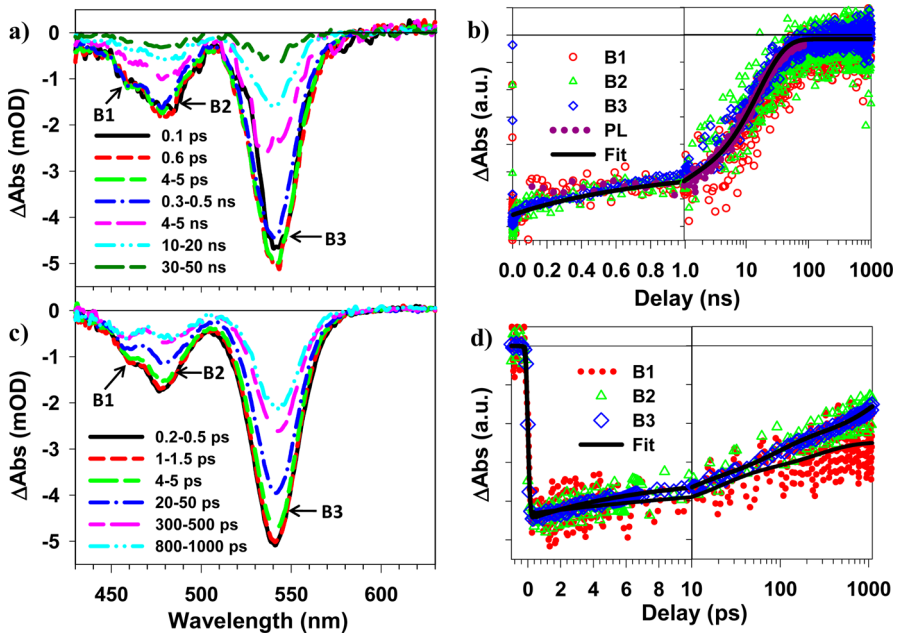

Figure 2. TA spectra and kinetics of DIRs (a, b) and DIR-BQ complexes (c, d). (a) TA spectra of DIRs from 0.1 ps to 50 ns after 540 nm excitation. (b) Kinetics of B1 (red circles), B2 (green triangles), and B3 (blue diamonds) bleaches shown in panel (a), time-resolved PL decay (purple dotted line, measured at 532−650 nm with 400 nm excitation), and multiple-exponential fits (black solid lines). (c) TA spectra of DIR-BQ complexes from 0.2 to 1000 ps after 540 nm excitation. (d) Kinetics of B1 (red dots), B2 (green triangles), and B3 (blue diamonds) bleaches shown in panel (c) and multiexponential fits (black solid lines).

Previous TA studies of group II−VI QDs[19,92,99−101] or nanorods[36,49,88,102] have shown that the bleach in exciton bands can be attributed to the state-filling of the CB electron levels with negligible contribution of VB hole-filling signals.[99,103,104] The lack of VB hole state-filling signal is generally attributed to higher density and degeneracy of the hole levels in II−VI semiconductors.[99,103,104] TA study of DIR−methyl viologen (MV^{2+}) complexes, in which CB electrons are selectively transferred to the MV^{2+} acceptor (Figure S4a and S4b in the Supporting Information), shows that the exciton bleach features in the DIR TA spectra are also caused exclusively by state-filling of the CB electron level associated with the transition, and they can be used to follow the kinetics of CB electrons.[19,36,88,92,100,101,105]

The kinetics of B2 and B3 after 540 nm excitation are shown in Figure 2b, along with the band edge exciton PL decay kinetics. It can be seen that these kinetics agree well with each other and can be fitted by the same two-exponential decay function (see Table S4 in the Supporting Information). The agreement of the B2 and B3 kinetics indicates that these transitions involve the same electron level, which suggests that the lowest energy CB electron level in the DIR is delocalized between the CdSe core and CdS bulb, as depicted in Scheme 1b. The observed quasi-type II band alignment is consistent with the electronic structure of CdSe/CdS core/shell QDs of similar core and shell dimensions.[92−96] The agreement of the TA and PL kinetics indicates that the lowest energy VB hole in the CdSe core decays mainly through recombination with the electron, which is consistent with their spatial separation from the nanocrystal surface. From the amplitude-weighted average lifetime of τ_{av} of 13.0 ± 0.16 ns (see Table S4) and the average PL QY of 48.7(±2.0)% under 540 nm excitation, an average radiative recombination time constant τ_r is estimated to be 26.7 ns using $\tau_r = \tau_{av}/QY$. This radiative lifetime is comparable to CdSe/CdS core/shell QDs, consistent with electron delocalization into CdS and a quasi-type II band alignment in the bulb region.[106]

In addition to B2 and B3, Figure 2a also shows a small apparent bleach feature at ~455 nm, near the B1 transition of the CdS rod. In free QDs, B1 bleach kinetics agree well with B2 and B3 bleach recovery. This suggests two possible origins for the small B1 feature. It may result from the state-filling-induced bleach of the B1 transition, which would suggest that the lowest energy CB electron level also extends into the CdS rod. Alternatively, it may be a Stark effect signal generated by the lowest energy exciton, which leads to derivative-like features of the B1 transition.

To differentiate these two possibilities, we have also measured TA spectra in DIR−benzoquinone (BQ) complexes (Figure 2C) at 540 nm excitation. BQ is chosen because it is a well-known electronic acceptor whose reduced form does not absorb in the visible region.[36,88,92,107,108] Furthermore, the electron-transfer (ET) rate in DIR-BQ complexes is relatively slow, so that we can accurately compare the bleach recovery kinetics of B1, B2, and B3 transitions. Similar comparison is not possible in DIR-MV^{2+} complexes due to much faster ET rates. As shown in Figure 2c, both B2 and B3 decay much faster in DIR−BQ complexes than in free DIRs, consistent with the expected ET from DIR to BQ.

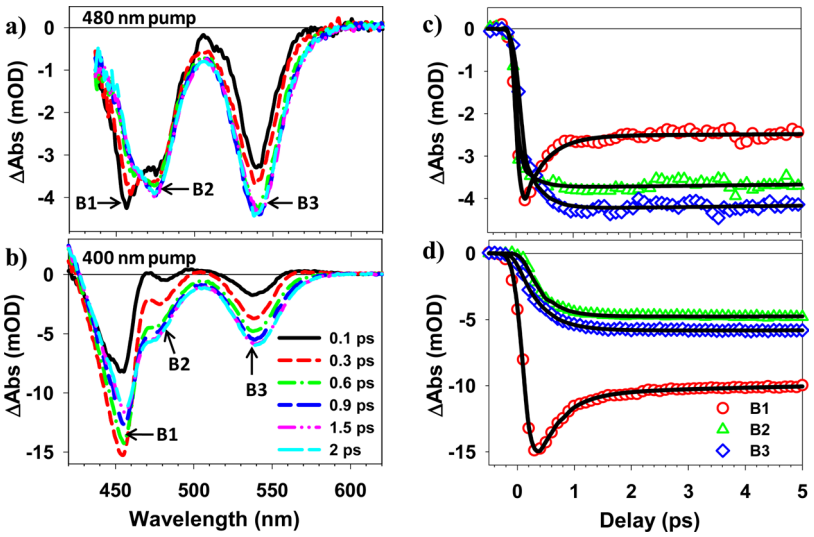

Figure 3. TA spectra and kinetics of DIRs at early delay time (0−5 ps) after 480 and 400 nm excitation. TA spectra at indicated delay times (a, c) and formation and decay kinetics of B1, B2, and B3 bleach (b and d) after 480 nm (a, b) and 400 nm (c, d) excitation. The black solid lines in (b) and (d) are multiexponential fits according to a model described in the Supporting Information, and fitting parameters are listed in Table S3 (in the Supporting Information).

Comparison of the normalized B2 and B3 kinetics (Figure 2d) shows that they agree well with each other, suggesting that these transitions involved the same lowest energy electron levels, consistent with the assignment above. These recovery kinetics can be fitted with the same three-exponential decay function with a half-life of 312 ± 40 ps (Table S5 in the Supporting Information). It is also clear from Figure 2c and d that the B1 feature decays much less than B2 and B3 in DIR−BQ complexes. This suggests that this feature in the TA spectra of free DIR (under 540 nm excitation) can be attributed to the derivative-like feature in the B1 transition caused by the Stark effect of (or exciton−exciton interaction with) the lowest energy exciton.[99,104] In DIR−BQ complexes, the decay of the lowest energy electron forms a charge-separated state, which also causes a Stark effect signal of the B1 transition, leading to negligible decay of the B1 feature.[19,36,49,88,92,109] Furthermore, the TA spectrum in Figure 2a can be well represented by the sum of Stark effect signals in B1, B2, and B3 and state-filling signals in B2 and B3, as shown in Figure S5, which further supports the proposed assignment.

Excitation Wavelength Dependent Exciton Relaxation Dynamics. We first examine the exciton dynamics with excitation pulses centered at 480 nm. As can be seen from the spectral overlap between the pump pulse and the absorption spectrum of DIRs shown in Figure S6 (in the Supporting Information), this pump pulse selectively excites the bulb-like CdS shell region (B2 transition) with a minor contribution by the CdS rod (B1 transition). The TA spectra within the first 2 ps after 480 nm excitation (Figure 3a) show bleach features at B1 (~455 nm), B2 (~480 nm), and B3 (~540 nm) transitions. The formation and decay kinetics of these features and their multiple-exponential fits are shown in Figure 3d. The details of the fit are described in the Supporting Information, and the fitting parameters are shown in Table S3. Both B2 and B3 bleach bands contain a nearly instantaneous formation component and a smaller growth component with time constants of 0.375 ± 0.060 and 0.403 ± 0.069 ps, respectively. The instantaneous formation of the B3 bleach upon excitation of the B2 band confirms that these transitions share the same CB electron level, consistent with the findings of 540 nm excitation discussed above. The B1 bleach shows an instrument response limited (<0.01 ps) formation time and a fast decay component with a time constant of 0.391 ± 0.051 ps, which agrees well with the formation time of the second growth component of B2 and B3 bleach features. This suggests that B1 bleach is formed by the direct excitation of the B1 transition and its decay leads to the formation of the second growth component of the B2 and B3 bleach. This exciton decay kinetics is further confirmed below with 400 nm excitation.

The evolution of TA spectra of DIRs within the first 2 ps after 400 nm excitation is shown in Figure 3c. Although both the CdSe seed and CdS bulb region have higher energy transitions at this excitation wavelength, the absorption is dominated by the CdS rod due to its much larger volume, leading to a selective generation of excitons in the CdS rod. The TA spectra show a partial decay of B1 bleach and the corresponding growth of B2 and B3 features. The formation and decay kinetics of these features within the first 5 ps are compared in Figure 3d. They can be well fit by multiexponential functions according to equations S2, S3, and S4, and the fitting parameters are listed in Table S3 in the Supporting Information. The B1 bleach shows a formation time of 0.066 ± 0.015 ps, which can be attributed to an electron relaxation process from the

initially excited 1π to the 1σ CB level within the CdS NR.[88] The decay of B1 bleach contains a fast component with 53% of its amplitude and a time constant of 0.422 $\pm$ 0.052 ps and a slow component on the nanosecond and longer time scale (see below). B3 kinetics exhibits a single-exponential rise time constant of 0.407 $\pm$ 0.041 ps. At early decay times, the signal at the B2 spectral region consists of the bleach of the B2 band as well as the red-shifted absorption of the B1 band that has been attributed to the effect of hot (1Π) exciton on the transition energy of the 1Σ exciton. Taking both features into account, the fit reveals a B2 bleach formation time constant of 0.387 $\pm$ 0.057 ps. The agreement between the time constants for B1 bleach decay and B2 and B3 bleach formation suggests that 53% of the initial excitation in the CdS rod decays to form the B2 and B3 bleach features in the bulb and seed regions.

TA spectra and kinetics of DIRs at longer delay times (5 ps to 1 μs) after 400 nm excitation are shown in Figure 4. There are no apparent interchanges between B1, B2, and B3 features, and their decay kinetics can be well described by multiexponential functions with fitting parameters listed in Table S4. B3 kinetics is the same as that measured with 540 nm excitation and can be fit by the same parameters. This suggests that the decay kinetics of excitons that are responsible for the B3 bleach feature is independent of their generation processes (*via* direct excitation or relaxation from higher energy exciton states). The half-lives are 22.5($\pm$1.7), 21.0($\pm$1.6), and 8.34 ($\pm$0.31) ns for B1, B2, and B3, respectively. Compared to B3 bleach, considerably longer lifetimes are observed for the B1 and B2 bleach features. The different decay times observed for these features suggest that the initial exciton generated on the CdS rod can decay into three distinct long-lived states in the DIR, and these states do not convert into each other after the first picosecond.

Assignment of Three Long-Lived Exciton States. It is clear from the TA study that the lowest energy exciton (X3) generated with 540 nm excitation involves a hole in the CdSe core and an electron that is delocalized into the CdS shell in the bulb region, which is shown in Scheme 1a and b. As a result, the presence of this exciton leads to the bleach of both B2 and B3 transitions, as shown in Figure 2a. The B2 bleach amplitude in the TA spectra is smaller than B3 bleach, whereas they have comparable absorption cross sections in the static absorption spectrum. This suggests that in the X3 exciton state, despite the quasi-type II band alignment, the electron is not delocalized throughout the entire bulb and is confined in the CdS shell that is close to the CdSe core. It should be noted that similar core-localized excitons have been observed in CdSe/CdS quasi-type II core/shell QDs, in which the localization of holes to the CdSe core leads to an increase of the bleach of lowest energy transition even though the electron is directly excited to the lowest energy CB level.[92] This

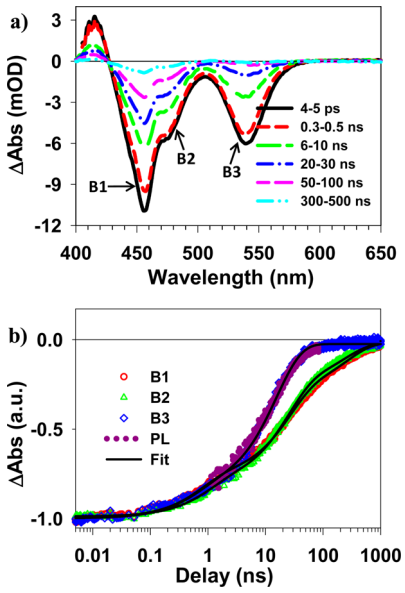

Figure 4. TA spectra and kinetics of DIR at 5 ps to 1 μs after 400 nm excitation. (a) TA spectra of DIRs at indicated delay time windows. (b) Kinetics of B1 (red circles), B2 (green triangles), and B3 (blue diamonds) features shown in Figure 2a, PL decay kinetics (purple dotted line) of DIRs measured at 532–675 nm after 400 nm excitation, and multiexponential fits (black solid lines).

phenomenon is attributed to a Coulomb-attraction-induced electron localization process to be elaborated below.

The PLE spectrum (Figure 1b) shows that excitation at higher energy also leads to X3 exciton emission. However, not all higher energy excitons relax to the X3 state, suggesting the presence of other exciton decay pathways. Direct excitation of the bulb region (B2 transition) leads to the bleach of B2 and B3, as shown in Figure 3a. Formation of B3 bleach is indicative of the presence of X3 excitons. The TA spectra show a larger relative amplitude of B2 than B3 bleach features compared to the TA spectrum of X3 (Figure 2a), suggesting that 480 nm excitation generates other species in addition to the X3 exciton. To obtain the spectrum of the yet-to-be-assigned exciton feature, we can subtract the total spectrum by the contribution of X3. This subtraction procedure avoids the need to model the exact line shape of TA bleach associated with excitons, which is often complicated due to exciton fine structure[110] and biexciton interaction induced spectral shifting.[99,104] In Figure 5a, we plotted the average TA spectra at 5–10 ps after 400 nm (black solid line), 480 nm (purple dashed line), and 540 nm (blue dotted line) excitation. They have been normalized at the B3 bleach peak. Because 540 nm excitation creates X3 excitons, we assign the difference spectrum between the TA spectra of 480 and 540 nm excitation (green triangles in Figure 5a) to X2 excitons. Similarly, the difference spectrum between 400 and 480 nm excited TA spectra (red circles in Figure 5a) is attributed to X1 excitons. We note that a small contribution of X1

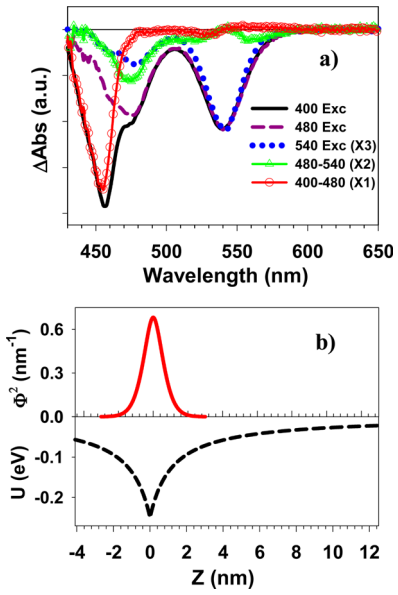

Figure 5. (a) Averaged TA spectra of DIRs from 5 to 10 ps after 400 nm (black solid line), 480 nm (purple dashed line), and 540 nm (blue dotted line) excitations. The spectrum measured at 540 nm excitation is assigned to X3 excitons. The difference spectrum between 480 and 540 nm excitation (green triangles) is assigned to X2 excitons, and the difference spectrum between 400 and 480 nm excitation (red circles) is assigned to X1 excitons. (b) 1D electron−hole Coulomb potential profile (black dashed line) and the corresponding electron probability density of the 1D exciton ground state (red solid line) as a function of electron−hole distance along the DIR long axis (*Z*). See main text for details.

exciton to the TA spectrum of 480 nm excitation has also been subtracted to yield the X2 exciton spectrum shown in Figure 5a.

As shown in Figure 5a, the X2 exciton spectrum shows a bleach of the B2 band with small derivative-like features at B3 and B1 transitions. The latter can result from subtraction errors and/or the Stark effect of the X2 exciton on B1 and B2 transitions. In the subtraction procedure we have assumed all B3 bleach is caused by X3 excitons. According to the PLE spectrum (Figure 1b), the band edge emission QY at 480 nm excitation is only 84% of that at 540 nm excitation, suggesting that 84% and 16% of the excitons generated at 480 nm relax to X3 and X2 exciton states, respectively. Therefore, it is reasonable to assume that the majority of the B3 bleach amplitude in Figure 3a is caused by the presence the X3 exciton, although we cannot exclude a small contribution of the X2 exciton to B3 bleach. Despite this uncertainty, it is reasonable to conclude that the spatial distribution of the electrons associated with the X2 exciton is different from that of X3 exciton, such that the former does not lead to or has much smaller contribution to the state-filling-induced bleach in the B3 transition. In light of the quasi-type II band alignment between CdSe/CdS, we propose that one way to satisfy this requirement is to have the electron strongly bound to a hole that is localized on a surface trap state, as depicted in Scheme 1a and b. Within this model, the initial excitation at 480 nm generates delocalized electrons and holes in the CdSe/CdS bulb region, which leads to instantaneous formation of B2 and B3 bleach observed in Figure 3a. The localization of holes to the CdSe core, driven by a large valence band offset between CdSe and CdS, forms the X3 exciton, in which the conduction band electron is also localized near the CdSe core. In competition with this process, holes can also be trapped on the surface trap states of the CdS bulb, which localizes the electrons near the trapped holes, forming the X2 exciton.

Similarly, the X1 exciton spectrum is well represented by the bleach of the B1 transition, with minor derivative-like features at B2 and B3 transitions. Initial excitation at 400 nm generates delocalized electrons and holes on the CdS rod. Because of the smaller quantum confinement energy of both valence band holes and conduction band electrons in the bulb compared to the rod, these carriers can be transferred into the bulb region, which can then form X3 and X2 excitons similar to the dynamics observed by direct excitation at 480 nm. In competition with this process, the valence band holes can also be trapped on the CdS rod surface, which localizes the electrons and forms the X1 exciton, as depicted in Scheme 1b. In the X1 exciton state, the electrons are located in the conduction band of the CdS rod, which accounts for the B1 bleach, but they are bound to the trapped holes. The decay of the X1 and X3 excitons can be directly monitored by B1 and B3 bleach recovery kinetics, which are shown in Table S4. The X2 exciton decay kinetics can be obtained by subtracting the contribution of the X3 exciton to the B2 bleach, which is also listed in Table S4. The long and uncorrelated lifetime of X1, X2, and X3 excitons and the lack of interconversion between these species after the initial ultrafast hole localization processes (Figure 4) suggest that X1 and X2 excitons are strongly bound due to either large Coulomb binding energy and/or deep hole trap energy.

It is worth noting that the TA spectra of DIR under 400 and 480 nm excitations show similar relative amplitudes of B2 and B3 bleach features. This implies that there is a constant partitioning factor between holes localizing in the core and on the bulb surface, regardless of whether they are initially generated *via* direct excitation (in the case of 480 nm pump) or transfer from the CdS rod (in the case of 400 nm pump). This partitioning factor is determined by the relative rates of hole trapping to the shell surface and hole transfer to the core in the quasi-type II CdSe core/CdS shell structure. From the initial decay (53%) of the B1 bleach at 400 nm excitation and the yield (46%) of hole capture to CdSe core determined by PLE, the branching ratio of forming the long-lived X1, X2, and X3 exciton states at 400 nm excitation can be estimated

to be 47%, 7%, and 46%, respectively. This X2:X3 branching ratio (13:87) is consistent with the value for 480 nm excitation (16:84) that we have estimated above from the PLE spectrum.

The proposed model of X1 and X2 excitons requires large binding energies and spatially localized electron and hole wave functions, which can arise from the dielectric confinement effect in 1D nanorods. Because the motion of electrons and holes in the radial direction of NRs is much faster than that in the axial direction, it is reasonable to average the electron−hole Coulomb interaction over the radial coordinates, yielding an effective 1D Coulomb potential along the axial direction.[81] Efros and co-workers have shown that the enhanced 1D Coulomb interaction in CdSe NRs leads to the formation of strongly bound 1D excitons with a large electron−hole binding energy of over 0.15 eV and small exciton radius of 1.6 nm.[81] According to this model, the 1D Coulomb potential profile is[81]

$$U(z) = -e^2/\kappa_m(|z| + \rho_{eff}) \quad (1)$$

where e is the electron charge, κ_m is the dielectric constant of the medium, and $|z|$ is the distance between electron and hole. ρ_{eff} is the effective screening length, which is assumed to be $0.7a$ (a is the radius of the NR), the same as the value determined for CdSe NRs.[81] At $|z| = 0$, we have $U_0 = U(0) = -e^2/\kappa_m\rho_{eff}$, the depth of the Coulomb potential well. Therefore eq 1 can be simplified to

$$U(z) = U_0\rho_{eff}/(|z| + \rho_{eff}) \quad (2)$$

Using the κ_m (3.2) of chloroform[111] and a ρ_{eff} of 1.21 nm, the depth of potential well U_0 is calculated to be 0.25 eV for the CdS rod. The Coulomb potential profile as a function of e−h separation distance (z) is shown in Figure 5b, lower panel. The wave functions of 1D excitons confined in this potential well are Whittaker-type functions, $\Phi(z) \propto W_{\alpha,1/2}(\bar{z})$, with $\bar{z} = 2(|z| + \rho_{eff})/(a_{1D}\alpha)$. Here $a_{1D} = e^2\kappa_m/\hbar^2\mu$, where $\hbar$ is the reduced Plank constant and μ the reduced mass of the electron−hole pair.[81,112] The ground state is the first even state satisfying the boundary condition $d\Phi(z)/dz\ (z = 0) = 0$. Solving this equation gives the first root at $\alpha = 0.185$. The resulting probability density distribution is shown in Figure 5b, upper panel. It shows that the excitons are highly localized, with 87.6% of the total density found within ±1 nm from the hole. Although this simple calculation is for axially delocalized electrons and holes in CdS nanorods and may differ from the electrons that are bound to holes that are trapped at the CdS surface or CdSe core, their much smaller dimension compared to the rod length provides qualitative support for spatially separated and localized X1, X2, and X3 excitons in the CdSe/CdS nanorods.

Charge Separation from Three Types of Excitons. To further examine the nature of X1, X2, and X3 excitons, we have also investigated charge separation properties of DIR−BQ complexes. The TA spectra of DIR−BQ complexes at indicated delay times after 400 nm excitation are shown in Figure 6a, upper (0−1000 ps) and lower (1−2000 ns) panels. They show the initial formation of B1, B2, and B3 bleaches within the first picosecond, the same as in free DIRs, indicating the formation of X1, X2, and X3 excitons. All three bleach features recover faster than free DIRs (Figure 4), which can be attributed to electron transfer to BQ. The decay of the exciton bleach leads to the formation of much weaker TA features that are derivatives of the B1, B2, and B3 exciton bands and can be assigned to the TA spectrum of charge-separated states (CS or DIR^+-BQ^-). Similar spectral evolution on a much faster time scale can be observed in DIR−MV^{2+} complexes (Figure S3) and in other QD-electron-acceptor complexes.[109,113,114]

The spectral evolution from excited NR to CS features is completed at ∼100 ns, indicating the completion of the exciton dissociation process. The decay of the charge-separated state TA spectral features on the 100−3000 ns time scale can be attributed to the charge recombination process. This can be further illustrated by the comparison of normalized kinetics of B1, B3, and CS shown in Figure 6b. The CS kinetics reflects the TA signal between 460 and 470 nm, which switches from negative state-filling-induced bleach in the excited NR to a positive Stark effect feature in the charge-separated states.[88] The kinetics of this CS peak is inverted and scaled to compare with B1 and B3 in Figure 6b, and all of them have been normalized to have the same value at 100 ns. Indeed, after ∼100 ns, all three features decay in the same way and can be attributed to charge recombination. It should also be noted that the B1 and B3 bleach decay kinetics do not agree with those in free DIRs (see the comparison in Figure S7) and cannot be assigned to the presence of free DIRs in the assembly of DIR−BQ complexes. It is important to point out that the CS states resulting from the dissociation of these three excitons may have different spectra and recombination rates. However, due to their small signal amplitudes, these different charge-separated states cannot be differentiated in this measurement. As a result, we can assume that there is one CS state spectrum, whose decay reflects the average charge recombination time.

Because of the overlap of X1, X2, X3, and CS TA spectra, a quantitative extraction of charge separation and recombination kinetics requires the fitting of the TA spectra in Figure 6a by the time-dependent contributions of these spectral components. Details of the fitting process and quality of the fit are provided in the Supporting Information (Figure S7). The time-dependent coefficients for the former and the latter are charge separation and recombination kinetics, respectively, which are shown in Figure 6c.

The kinetics of X3 exciton recovery is identical to that measured at 540 nm excitation, showing a half-life of 312 ± 40 ps. The kinetics of X1 and X2 exciton

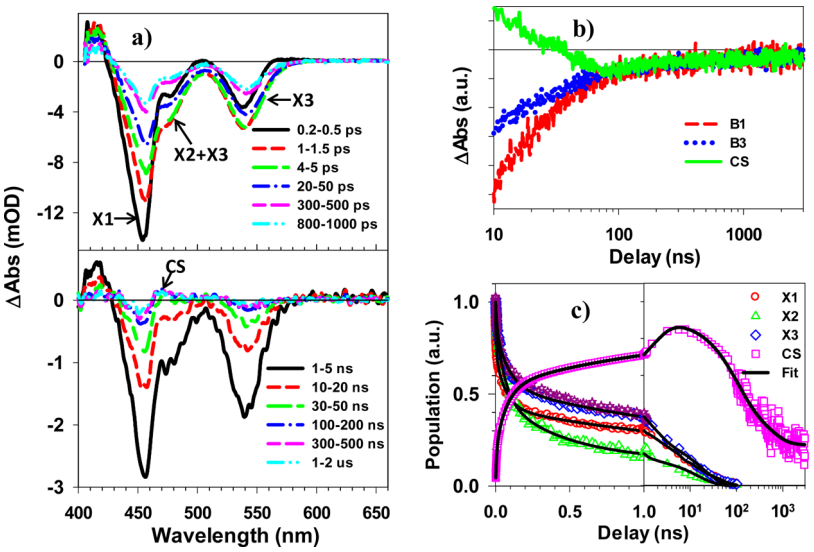

Figure 6. TA spectra and kinetics of DIR−BQ complexes measured at 400 nm excitation. (a) TA spectra of DIR−BQ complexes at 0.2 to 1000 ps (upper panel) and 1 to 2000 ns (lower panel). (b) Comparison of kinetics of B1 and B3 and CS (labeled in panel a) features from 1 to 3000 ns. The CS signal has been inverted, and all signals have been normalized to the same value at 100−3000 ns. (c) Time-dependent populations of X1 (red circles), X2 (green triangles), X3 (blue diamonds), and charge-separated state (CS, pink squares) from 0 to 3000 ns and their multiexponential fits (black lines). Also shown for comparison is the X3 exciton dissociation kinetics measured at 540 nm excitation (purple stars).

dissociation can also be fitted to multiexponential decays (see Supporting Information for details), and the fitting parameters are listed in Table S5. The half-life times are 63.5(±21) and 112(±49) ps for X1 and X2, respectively. The exciton dissociation rates show a trend of X1 > X2 > X3, showing the slowest ET rate for the X3 exciton. This is consistent with the electron distribution of the X3 exciton, which is largely localized in and near the CdSe core, away from the CdS surface, reducing its electronic coupling with the acceptor. The dissociation rate for X1 is similar to that in CdS NR−BQ complexes (~90 ps),[88] although a quantitative comparison is difficult, as the rate likely depends on rod length and the number of absorbed BQ molecules.

The time-dependent population of the charge-separated state can be well fit to a three-exponential function, from which a half-life of 155 ± 27 ns for charge recombination is extracted. The slow recombination in DIR−BQ complexes is a result of hole localization: they are either localized in the core (X3) or localized in the deep-trapping center on CdS surfaces (X1, X2). This is consistent with previous reported slow charge recombination in systems with core-localized or surface-trapped holes, such as CdSe/ZnS,[109] CdTe/CdSe,[19] and CdSe/CdS[92] core/shell QDs or CdS NRs.[88]

CONCLUSION

In conclusion, using CdSe/CdS dot-in-rod 1D nanorods as a model system, we have studied exciton formation, relaxation, and dissociation dynamics in 1D nanorod heterostructures by transient absorption spectroscopy. CdSe/CdS nanorods were prepared by a seeded growth method, consisting of a CdSe seed surrounded by a CdS shell and a CdS rod. A difference in the quantum confinement energy in the CdS shell and rod region (caused by the larger diameter in the former) and bulk band edge positions in CdSe and CdS leads to three distinct optical absorption features in the DIR with their lowest energy transitions, labeled as B1, B2, and B3 in Scheme 1b. We showed that excitation at the B3 transition led to the bleach of B2 and B3 transitions. Because the B3 transition directly generates the band edge exciton (X3) with a hole localized in the CdSe valence band and electron in the lowest energy conduction band level of the DIR, the formation of B2 bleach suggests that the electron level is delocalized in the CdSe seed/CdS shell region, indicating a quasi-type II band alignment.

Excitation of the B2 transition, promoting an electron from the lowest energy VB of the CdS shell to the lowest energy delocalized CB level of the CdSe seed/CdS shell region, leads to the bleach of the B2 and B3 transitions and a larger amplitude of the B2 bleach compared to the TA spectrum of the X3 exciton. This suggests the formation of the X2 exciton (with bleach of the B2 band) in addition to the X3 excitons. Excitation at B1 generates excitons at the CdS rod region: 47% of the excitons relax to form X1 excitons, with electrons in the conduction band of the CdS rod (giving rise to the B1 bleach); 7% and 46% of the remaining excitons relax to X2 and X3 states, respectively. These exciton states are long-lived, with half-lives of 22.5(±1.7) ns, 32.1(±2.2) ns, and 8.34(±0.31) ns for X1, X2, and X3 excitons, respectively. The lack of interconversion between these exciton states suggests that they are spatially separated and/or strongly bound.

We propose that in the X3 exciton state the electron is localized in and near the CdSe seed due to strong Coulomb attraction by the CdSe confined hole, despite the quasi-type II band alignment. The formation of the X2 state is driven by hole trapping on the CdS shell, which localizes the electrons to the surface-trapped holes. The hole-driven localization process and strong electron−hole interaction form spatially separated X2 and X3 excitons despite their common electron level in this 1D material with quasi-type II band alignment. Similarly, the X1 exciton state is formed by hole trapping on the CdS rod, which localizes the electron and separates X1 from X2 and X3 excitons. The hole-driven exciton localization process occurs with a time constant of ~0.4 ps, likely limited by the hole transfer/trapping rates due to their larger effective mass. The partition between these exciton states is controlled by the relative rates of hole localization and trapping. To provide further support of the proposed exciton identity, we have also studied their dissociation kinetics in DIR−benzoquinone complexes. In the presence of the electron acceptor, we showed that these excitons were shorter lived due to electron transfer to the acceptors and their electron transfer rates were different. The X3 excitons show the slowest dissociation rate, consistent with the proposed structure in which the electrons are localized near the CdSe seed further away from the CdS surface compared to the X1 and X2 excitons.

Our results demonstrate that in 1D nanorod heterostructures the fate of excitons is determined by not only the overall band alignment of the components but also the dynamics of exciton relaxation. The latter can be strongly influenced by carrier trapping induced exciton localization due to strong electron−hole interaction in 1D materials. The distinct spatial locations of these excitons have an important effect on their application as light-harvesting materials for solar energy conversion.

METHODS/EXPERIMENTAL SECTION

CdSe−CdSe DIRs were prepared by a standard seeded growth procedure starting with a 2.35 nm (diameter) CdSe QD seed.[23,24] DIR−BQ complexes were prepared by adding BQ powder to a DIR chloroform solution followed by sonication. DIR−MV^{2+} complexes were prepared by adding several drops of concentrated MV^{2+} methanol solution to a DIR chloroform solution followed by sonication. All samples were filtered through 2 μm filters before TA experiments to remove undissolved molecules and to minimize light scattering. Details of sample preparations and TA spectrometer setups are provided in the Supporting Information.

Conflict of Interest: The authors declare no competing financial interest.

Acknowledgment. This work was funded by the U.S. Department of Energy, Office of Basic Energy Sciences, Solar Photochemistry Program (DE-FG02-12ER16347).

Supporting Information Available: Synthesis procedure, additional transient absorption spectra and kinetics, fitting procedures, and fitting parameters. This material is available free of charge *via* the Internet at http://pubs.acs.org.

REFERENCES AND NOTES

1. Milliron, D. J.; Hughes, S. M.; Cui, Y.; Manna, L.; Li, J.; Wang, L.-W.; Alivisatos, A. P. Colloidal Nanocrystal Heterostructures with Linear and Branched Topology. *Nature* **2004**, *430*, 190–195.
2. Reiss, P.; Protière, M.; Li, L. Core/Shell Semiconductor Nanocrystals. *Small* **2009**, *5*, 154–168.
3. Hines, M. A.; Guyot-Sionnest, P. Synthesis and Characterization of Strongly Luminescing ZnS-Capped CdSe Nanocrystals. *J. Phys. Chem.* **1996**, *100*, 468–471.
4. Dabbousi, B. O.; Rodriguez-Viejo, J.; Mikulec, F. V.; Heine, J. R.; Mattoussi, H.; Ober, R.; Jensen, K. F.; Bawendi, M. G. (CdSe)ZnS Core−Shell Quantum Dots: Synthesis and Characterization of a Size Series of Highly Luminescent Nanocrystallites. *J. Phys. Chem. B* **1997**, *101*, 9463–9475.
5. Peng, X.; Schlamp, M. C.; Kadavanich, A. V.; Alivisatos, A. P. Epitaxial Growth of Highly Luminescent CdSe/CdS Core/Shell Nanocrystals with Photostability and Electronic Accessibility. *J. Am. Chem. Soc.* **1997**, *119*, 7019–7029.
6. Scholes, G. D. Controlling the Optical Properties of Inorganic Nanoparticles. *Adv. Funct. Mater.* **2008**, *18*, 1157–1172.
7. Shieh, F.; Saunders, A. E.; Korgel, B. A. General Shape Control of Colloidal CdS, CdSe, CdTe Quantum Rods and Quantum Rod Heterostructures. *J. Phys. Chem. B* **2005**, *109*, 8538–8542.
8. Smith, A. M.; Nie, S. Semiconductor Nanocrystals: Structure, Properties, and Band Gap Engineering. *Acc. Chem. Res.* **2009**, *43*, 190–200.
9. Kim, S.; Fisher, B.; Eisler, H.-J.; Bawendi, M. Type-II Quantum Dots: CdTe/CdSe(Core/Shell) and CdSe/ZnTe-(Core/Shell) Heterostructures. *J. Am. Chem. Soc.* **2003**, *125*, 11466–11467.
10. Ivanov, S. A.; Piryatinski, A.; Nanda, J.; Tretiak, S.; Zavadil, K. R.; Wallace, W. O.; Werder, D.; Klimov, V. I. Type-II Core/Shell CdS/ZnSe Nanocrystals: Synthesis, Electronic Structures, and Spectroscopic Properties. *J. Am. Chem. Soc.* **2007**, *129*, 11708–11719.
11. Alivisatos, P. The Use of Nanocrystals in Biological Detection. *Nat. Biotechnol.* **2004**, *22*, 47–52.
12. Xing, Y.; Chaudry, Q.; Shen, C.; Kong, K. Y.; Zhau, H. E.; Chung, L. W.; Petros, J. A.; O'Regan, R. M.; Yezhelyev, M. V.; Simons, J. W.; Wang, M. D.; Nie, S. Bioconjugated Quantum Dots for Multiplexed and Quantitative Immunohistochemistry. *Nat. Protoc.* **2007**, *2*, 1152–1165.
13. Michalet, X.; Pinaud, F.; Bentolila, L.; Tsay, J.; Doose, S.; Li, J.; Sundaresan, G.; Wu, A.; Gambhir, S.; Weiss, S. Quantum Dots for Live Vells, *in Vivo* Imaging, and Diagnostics. *Science* **2005**, *307*, 538–544.
14. Chan, W. C. W.; Nie, S. Quantum Dot Bioconjugates for Ultrasensitive Nonisotopic Detection. *Science* **1998**, *281*, 2016–2018.
15. Tessler, N.; Medvedev, V.; Kazes, M.; Kan, S.; Banin, U. Efficient Near-Infrared Polymer Nanocrystal Light-Emitting Diodes. *Science* **2002**, *295*, 1506–1508.
16. Coe, S.; Woo, W.-K.; Bawendi, M.; Bulovic, V. Electroluminescence from Single Monolayers of Nanocrystals in Molecular Organic Devices. *Nature* **2002**, *420*, 800–803.
17. Oron, D.; Kazes, M.; Banin, U. Multiexcitons in Type-II Colloidal Semiconductor Quantum Dots. *Phys. Rev. B* **2007**, *75*, 035330.
18. Klimov, V. I.; Ivanov, S. A.; Nanda, J.; Achermann, M.; Bezel, I.; McGuire, J. A.; Piryatinski, A. Single-Exciton Optical Gain in Semiconductor Nanocrystals. *Nature* **2007**, *447*, 441–446.

19. Zhu, H.; Song, N.; Lian, T. Wave Function Engineering for Ultrafast Charge Separation and Slow Charge Recombination in Type II Core/Shell Quantum Dots. *J. Am. Chem. Soc.* **2011**, *133*, 8762–8771.
20. Talapin, D. V.; Koeppe, R.; Götzinger, S.; Kornowski, A.; Lupton, J. M.; Rogach, A. L.; Benson, O.; Feldmann, J.; Weller, H. Highly Emissive Colloidal CdSe/CdS Heterostructures of Mixed Dimensionality. *Nano Lett.* **2003**, *3*, 1677–1681.
21. Halpert, J. E.; Porter, V. J.; Zimmer, J. P.; Bawendi, M. G. Synthesis of CdSe/CdTe Nanobarbells. *J. Am. Chem. Soc.* **2006**, *128*, 12590–12591.
22. Kudera, S.; Carbone, L.; Casula, M. F.; Cingolani, R.; Falqui, A.; Snoeck, E.; Parak, W. J.; Manna, L. Selective Growth of PbSe on One or Both Tips of Colloidal Semiconductor Nanorods. *Nano Lett.* **2005**, *5*, 445–449.
23. Talapin, D. V.; Nelson, J. H.; Shevchenko, E. V.; Aloni, S.; Sadtler, B.; Alivisatos, A. P. Seeded Growth of Highly Luminescent CdSe/CdS Nanoheterostructures with Rod and Tetrapod Morphologies. *Nano Lett.* **2007**, *7*, 2951–2959.
24. Carbone, L.; Nobile, C.; De Giorgi, M.; Sala, F. D.; Morello, G.; Pompa, P.; Hytch, M.; Snoeck, E.; Fiore, A.; Franchini, I. R.; *et al*. Synthesis and Micrometer-Scale Assembly of Colloidal CdSe/CdS Nanorods Prepared by a Seeded Growth Approach. *Nano Lett.* **2007**, *7*, 2942–2950.
25. Kirsanova, M.; Nemchinov, A.; Hewa-Kasakarage, N. N.; Schmall, N.; Zamkov, M. Synthesis of ZnSe/CdS/ZnSe Nanobarbells Showing Photoinduced Charge Separation. *Chem. Mater.* **2009**, *21*, 4305–4309.
26. Koo, B.; Korgel, B. A. Coalescence and Interface Diffusion in Linear CdTe/CdSe/CdTe Heterojunction Nanorods. *Nano Lett.* **2008**, *8*, 2490–2496.
27. Kumar, S.; Jones, M.; Lo, S. S.; Scholes, G. D. Nanorod Heterostructures Showing Photoinduced Charge Separation. *Small* **2007**, *3*, 1633–1639.
28. Giblin, J.; Kuno, M. Nanostructure Absorption: A Comparative Study of Nanowire and Colloidal Quantum Dot Absorption Cross Sections. *J. Phys. Chem. Lett.* **2010**, *1*, 3340–3348.
29. Giblin, J.; Syed, M.; Banning, M. T.; Kuno, M.; Hartland, G. Experimental Determination of Single CdSe Nanowire Absorption Cross Sections through Photothermal Imaging. *ACS Nano* **2010**, *4*, 358–364.
30. Carey, C. R.; LeBel, T.; Crisostomo, D.; Giblin, J.; Kuno, M.; Hartland, G. V. Imaging and Absolute Extinction Cross-Section Measurements of Nanorods and Nanowires through Polarization Modulation Microscopy. *J. Phys. Chem. C* **2010**, *114*, 16029–16036.
31. Manna, L.; Scher, E. C.; Li, L.-S.; Alivisatos, A. P. Epitaxial Growth and Photochemical Annealing of Graded CdS/ZnS Shells on Colloidal CdSe Nanorods. *J. Am. Chem. Soc.* **2002**, *124*, 7136–7145.
32. Mokari, T.; Banin, U. Synthesis and Properties of CdSe/ZnS Core/Shell Nanorods. *Chem. Mater.* **2003**, *15*, 3955–3960.
33. Htoon, H.; Hollingsworth, J. A.; Dickerson, R.; Klimov, V. I. Effect of Zero- to One-Dimensional Transformation on Multiparticle Auger Recombination in Semiconductor Quantum Rods. *Phys. Rev. Lett.* **2003**, *91*, 227401.
34. Htoon, H.; Hollingworth, J.; Malko, A.; Dickerson, R.; Klimov, V. Light Amplification in Semiconductor Nanocrystals: Quantum Rods *versus* Quantum Dots. *Appl. Phys. Lett.* **2003**, *82*, 4776.
35. Robel, I.; Bunker, B. A.; Kamat, P. V.; Kuno, M. Exciton Recombination Dynamics in CdSe Nanowires: Bimolecular to Three-Carrier Auger Kinetics. *Nano Lett.* **2006**, *6*, 1344–1349.
36. Zhu, H.; Lian, T. Enhanced Multiple Exciton Dissociation from CdSe Quantum Rods: The Effect of Nanocrystal Shape. *J. Am. Chem. Soc.* **2012**, *134*, 11289–11297.
37. Hu, J.; Li, L.-s.; Yang, W.; Manna, L.; Wang, L.-W.; Alivisatos, A. P. Linearly Polarized Emission from Colloidal Semiconductor Quantum Rods. *Science* **2001**, *292*, 2060–2063.
38. Hadar, I.; Hitin, G. B.; Sitt, A.; Faust, A.; Banin, U. Polarization Properties of Semiconductor Nanorod Heterostructures: From Single Particles to the Ensemble. *J. Phys. Chem. Lett.* **2013**, 502–507.
39. Sitt, A.; Salant, A.; Menagen, G.; Banin, U. Highly Emissive Nano Rod-in-Rod Heterostructures with Strong Linear Polarization. *Nano Lett.* **2011**, *11*, 2054–2060.
40. Wang, J.; Gudiksen, M. S.; Duan, X.; Cui, Y.; Lieber, C. M. Highly Polarized Photoluminescence and Photodetection from Single Indium Phosphide Nanowires. *Science* **2001**, *293*, 1455–1457.
41. Katz, D.; Wizansky, T.; Millo, O.; Rothenberg, E.; Mokari, T.; Banin, U. Size-Dependent Tunneling and Optical Spectroscopy of CdSe Quantum Rods. *Phys. Rev. Lett.* **2002**, *89*, 086801.
42. Li, L.-s.; Hu, J.; Yang, W.; Alivisatos, A. P. Band Gap Variation of Size- and Shape-Controlled Colloidal CdSe Quantum Rods. *Nano Lett.* **2001**, *1*, 349–351.
43. Deka, S.; Quarta, A.; Lupo, M. G.; Falqui, A.; Boninelli, S.; Giannini, C.; Morello, G.; De Giorgi, M.; Lanzani, G.; Spinella, C.; *et al*. CdSe/CdS/ZnS Double Shell Nanorods with High Photoluminescence Efficiency and Their Exploitation As Biolabeling Probes. *J. Am. Chem. Soc.* **2009**, *131*, 2948–2958.
44. Pisanello, F.; Martiradonna, L.; Spinicelli, P.; Fiore, A.; Hermier, J. P.; Manna, L.; Cingolani, R.; Giacobino, E.; De Vittorio, M.; Bramati, A. Dots in Rods as Polarized Single Photon Sources. *Superlattices Microstruct.* **2010**, *47*, 165–169.
45. Huang, M. H.; Mao, S.; Feick, H.; Yan, H.; Wu, Y.; Kind, H.; Weber, E.; Russo, R.; Yang, P. Room-Temperature Ultraviolet Nanowire Nanolasers. *Science* **2001**, *292*, 1897–1899.
46. Kazes, M.; Lewis, D. Y.; Ebenstein, Y.; Mokari, T.; Banin, U. Lasing from Semiconductor Quantum Rods in a Cylindrical Microcavity. *Adv. Mater.* **2002**, *14*, 317–321.
47. Tang, M. L.; Grauer, D. C.; Lassalle-Kaiser, B.; Yachandra, V. K.; Amirav, L.; Long, J. R.; Yano, J.; Alivisatos, A. P. Structural and Electronic Study of an Amorphous MoS3 Hydrogen-Generation Catalyst on a Quantum-Controlled Photosensitizer. *Angew. Chem., Int. Ed.* **2011**, *50*, 10203–10207.
48. Amirav, L.; Alivisatos, A. P. Photocatalytic Hydrogen Production with Tunable Nanorod Heterostructures. *J. Phys. Chem. Lett.* **2010**, *1*, 1051–1054.
49. Zhu, H.; Song, N.; Lv, H.; Hill, C. L.; Lian, T. Near Unity Quantum Yield of Light-Driven Redox Mediator Reduction and Efficient H2 Generation Using Colloidal Nanorod Heterostructures. *J. Am. Chem. Soc.* **2012**, *134*, 11701–11708.
50. Acharya, K. P.; Khnayzer, R. S.; O'Connor, T.; Diederich, G.; Kirsanova, M.; Klinkova, A.; Roth, D.; Kinder, E.; Imboden, M.; Zamkov, M. The Role of Hole Localization in Sacrificial Hydrogen Production by Semiconductor–Metal Heterostructured Nanocrystals. *Nano Lett.* **2011**, *11*, 2919–2926.
51. Berr, M.; Vaneski, A.; Susha, A. S.; Rodriguez-Fernandez, J.; Doblinger, M.; Jackel, F.; Rogach, A. L.; Feldmann, J. Colloidal CdS Nanorods Decorated with Subnanometer Sized Pt Clusters for Photocatalytic Hydrogen Generation. *Appl. Phys. Lett.* **2010**, *97*, 093108–3.
52. Brown, K. A.; Wilker, M. B.; Boehm, M.; Dukovic, G.; King, P. W. Characterization of Photochemical Processes for H2 Production by CdS Nanorod–[FeFe] Hydrogenase Complexes. *J. Am. Chem. Soc.* **2012**, *134*, 5627–5636.
53. Tongying, P.; Plashnitsa, V. V.; Petchsang, N.; Vietmeyer, F.; Ferraudi, G. J.; Krylova, G.; Kuno, M. Photocatalytic Hydrogen Generation Efficiencies in One-Dimensional CdSe Heterostructures. *J. Phys. Chem. Lett.* **2012**, 3234–3240.
54. Bang, J. U.; Lee, S. J.; Jang, J. S.; Choi, W.; Song, H. Geometric Effect of Single or Double Metal-Tipped CdSe Nanorods on Photocatalytic H2 Generation. *J. Phys. Chem. Lett.* **2012**, *3*, 3781–3785.
55. Müller, J.; Lupton, J. M.; Rogach, A. L.; Feldmann, J.; Talapin, D. V.; Weller, H. Monitoring Surface Charge Movement in Single Elongated Semiconductor Nanocrystals. *Phys. Rev. Lett.* **2004**, *93*, 167402.

56. Müller, J.; Lupton, J. M.; Lagoudakis, P. G.; Schindler, F.; Koeppe, R.; Rogach, A. L.; Feldmann, J.; Talapin, D. V.; Weller, H. Wave Function Engineering in Elongated Semiconductor Nanocrystals with Heterogeneous Carrier Confinement. *Nano Lett.* **2005**, *5*, 2044–2049.
57. Müller, J.; Lupton, J. M.; Rogach, A. L.; Feldmann, J.; Talapin, D. V.; Weller, H. Monitoring Surface Charge Migration in the Spectral Dynamics of Single CdSe/CdS Nanodot/Nanorod Heterostructures. *Phys. Rev. B* **2005**, *72*, 205339.
58. Kraus, R. M.; Lagoudakis, P. G.; Rogach, A. L.; Talapin, D. V.; Weller, H.; Lupton, J. M.; Feldmann, J. Room-Temperature Exciton Storage in Elongated Semiconductor Nanocrystals. *Phys. Rev. Lett.* **2007**, *98*, 017401.
59. Lupo, M. G.; Della Sala, F.; Carbone, L.; Zavelani-Rossi, M.; Fiore, A.; Lüer, L.; Polli, D.; Cingolani, R.; Manna, L.; Lanzani, G. Ultrafast Electron–Hole Dynamics in Core/Shell CdSe/CdS Dot/Rod Nanocrystals. *Nano Lett.* **2008**, *8*, 4582–4587.
60. Mauser, C.; Limmer, T.; Da Como, E.; Becker, K.; Rogach, A. L.; Feldmann, J.; Talapin, D. V. Anisotropic Optical Emission of Single CdSe/CdS Tetrapod Heterostructures: Evidence for a Wavefunction Symmetry Breaking. *Phys. Rev. B* **2008**, *77*, 153303.
61. Morello, G.; Della Sala, F.; Carbone, L.; Manna, L.; Maruccio, G.; Cingolani, R.; De Giorgi, M. Intrinsic Optical Nonlinearity in Colloidal Seeded Grown CdSe/CdS Nanostructures: Photoinduced Screening of the Internal Electric Field. *Phys. Rev. B* **2008**, *78*, 195313.
62. Steiner, D.; Dorfs, D.; Banin, U.; Della Sala, F.; Manna, L.; Millo, O. Determination of Band Offsets in Heterostructured Colloidal Nanorods Using Scanning Tunneling Spectroscopy. *Nano Lett.* **2008**, *8*, 2954–2958.
63. Luo, Y.; Wang, L.-W. Electronic Structures of the CdSe/CdS Core–Shell Nanorods. *ACS Nano* **2009**, *4*, 91–98.
64. Saba, M.; Minniberger, S.; Quochi, F.; Roither, J.; Marceddu, M.; Gocalinska, A.; Kovalenko, M. V.; Talapin, D. V.; Heiss, W.; Mura, A. Exciton-Exciton Interaction and Optical Gain in Colloidal CdSe/CdS Dot/Rod Nanocrystals. *Adv. Mater.* **2009**, *21*, 4942.
65. Sitt, A.; Sala, F. D.; Menagen, G.; Banin, U. Multiexciton Engineering in Seeded Core/Shell Nanorods: Transfer from Type-I to Quasi-Type-II Regimes. *Nano Lett.* **2009**, *9*, 3470–3476.
66. Borys, N. J.; Walter, M. J.; Huang, J.; Talapin, D. V.; Lupton, J. M. The Role of Particle Morphology in Interfacial Energy Transfer in CdSe/CdS Heterostructure Nanocrystals. *Science* **2010**, *330*, 1371–1374.
67. Lupo, M. G.; Zavelani-Rossi, M.; Fiore, A.; Polli, D.; Carbone, L.; Cingolani, R.; Manna, L.; Lanzani, G. Evidence of Electron Wave Function Delocalization in CdSe/CdS Asymmetric Nanocrystals. *Superlattices Microstruct.* **2010**, *47*, 170–173.
68. Lutich, A. A.; Mauser, C.; Da Como, E.; Huang, J.; Vaneski, A.; Talapin, D. V.; Rogach, A. L.; Feldmann, J. Multiexcitonic Dual Emission in CdSe/CdS Tetrapods and Nanorods. *Nano Lett.* **2010**, *10*, 4646–4650.
69. Mauser, C.; Da Como, E.; Baldauf, J.; Rogach, A. L.; Huang, J.; Talapin, D. V.; Feldmann, J. Spatio-temporal Dynamics of Coupled Electrons and Holes in Nanosize CdSe-CdS Semiconductor Tetrapods. *Phys. Rev. B* **2010**, *82*, 081306.
70. Morello, G.; Della Sala, F.; Carbone, L.; Manna, L.; Cingolani, R.; De Giorgi, M. Evidence for an Internal Field in CdSe/CdS Nanorods by Time Resolved and Single Rod Experiments. *Superlattices Microstruct.* **2010**, *47*, 174–177.
71. Zavelani-Rossi, M.; Lupo, M. G.; Tassone, F.; Manna, L.; Lanzani, G. Suppression of Biexciton Auger Recombination in CdSe/CdS Dot/Rods: Role of the Electronic Structure in the Carrier Dynamics. *Nano Lett.* **2010**, *10*, 3142–3150.
72. Krahne, R.; Morello, G.; Figuerola, A.; George, C.; Deka, S.; Manna, L. Physical Properties of Elongated Inorganic Nanoparticles. *Phys. Rep.* **2011**, *501*, 75–221.
73. Rainò, G.; Stöferle, T.; Moreels, I.; Gomes, R.; Kamal, J. S.; Hens, Z.; Mahrt, R. F. Probing the Wave Function Delocalization in CdSe/CdS Dot-in-Rod Nanocrystals by Time- and Temperature-Resolved Spectroscopy. *ACS Nano* **2011**, *5*, 4031–4036.
74. She, C.; Demortière, A.; Shevchenko, E. V.; Pelton, M. Using Shape to Control Photoluminescence from CdSe/CdS Core/Shell Nanorods. *J. Phys. Chem. Lett.* **2011**, *2*, 1469–1475.
75. Smith, E. R.; Luther, J. M.; Johnson, J. C. Ultrafast Electronic Delocalization in CdSe/CdS Quantum Rod Heterostructures. *Nano Lett.* **2011**, *11*, 4923–4931.
76. Xing, G.; Chakrabortty, S.; Ngiam, S. W.; Chan, Y.; Sum, T. C. Three-Photon Absorption in Seeded CdSe/CdS Nanorod Heterostructures. *J. Phys. Chem. C* **2011**, *115*, 17711–17716.
77. Rainò, G.; Stöferle, T.; Moreels, I.; Gomes, R.; Hens, Z.; Mahrt, R. F. Controlling the Exciton Fine Structure Splitting in CdSe/CdS Dot-in-Rod Nanojunctions. *ACS Nano* **2012**, *6*, 1979–1987.
78. Chakrabortty, S.; Xing, G.; Xu, Y.; Ngiam, S. W.; Mishra, N.; Sum, T. C.; Chan, Y. Engineering Fluorescence in Au-Tipped, CdSe-Seeded CdS Nanoheterostructures. *Small* **2011**, *7*, 2847–2852.
79. Yoskovitz, E.; Menagen, G.; Sitt, A.; Lachman, E.; Banin, U. Nanoscale Near-Field Imaging of Excitons in Single Heterostructured Nanorods. *Nano Lett.* **2010**, *10*, 3068–3072.
80. Kunneman, L. T.; Zanella, M.; Manna, L.; Siebbeles, L. D. A.; Schins, J. M. Mobility and Spatial Distribution of Photoexcited Electrons in CdSe/CdS Nanorods. *J. Phys. Chem. C* **2013**, *117*, 3146–3151.
81. Shabaev, A.; Efros, A. L. 1D Exciton Spectroscopy of Semiconductor Nanorods. *Nano Lett.* **2004**, *4*, 1821–1825.
82. Ekimov, A. I.; Hache, F.; Schanne-Klein, M. C.; Ricard, D.; Flytzanis, C.; Kudryavtsev, I. A.; Yazeva, T. V.; Rodina, A. V.; Efros, A. L. Absorption and Intensity-Dependent Photoluminescence Measurements on CdSe Quantum Dots: Assignment of the First Electronic Transitions. *J. Opt. Soc. Am. B* **1993**, *10*, 100–107.
83. Norris, D. J.; Sacra, A.; Murray, C. B.; Bawendi, M. G. Measurement of the Size Dependent Hole Spectrum in CdSe Quantum Dots. *Phys. Rev. Lett.* **1994**, *72*, 2612.
84. Puthussery, J.; Lan, A.; Kosel, T. H.; Kuno, M. Band-Filling of Solution-Synthesized CdS Nanowires. *ACS Nano* **2008**, *2*, 357–367.
85. Xu, X.; Zhao, Y.; Sie, E. J.; Lu, Y.; Liu, B.; Ekahana, S. A.; Ju, X.; Jiang, Q.; Wang, J.; Sun, H.; *et al.* Dynamics of Bound Exciton Complexes in CdS Nanobelts. *ACS Nano* **2011**, *5*, 3660–3669.
86. Hoang, T. B.; Titova, L. V.; Jackson, H. E.; Smith, L. M.; Yarrison-Rice, J. M.; Lensch, J. L.; Lauhon, L. J. Temperature Dependent Photoluminescence of Single CdS Nanowires. *Appl. Phys. Lett.* **2006**, *89*, 123123.
87. Saunders, A. E.; Ghezelbash, A.; Sood, P.; Korgel, B. A. Synthesis of High Aspect Ratio Quantum-Size CdS Nanorods and Their Surface-Dependent Photoluminescence. *Langmuir* **2008**, *24*, 9043–9049.
88. Wu, K.; Zhu, H.; Liu, Z.; Rodríguez-Córdoba, W.; Lian, T. Ultrafast Charge Separation and Long-Lived Charge Separated State in Photocatalytic CdS–Pt Nanorod Heterostructures. *J. Am. Chem. Soc.* **2012**, *134*, 10337–10340.
89. Shafran, E.; Borys, N. J.; Huang, J.; Talapin, D. V.; Lupton, J. M. Indirect Exciton Formation Due to Inhibited Carrier Thermalization in Single CdSe/CdS Nanocrystals. *J. Phys. Chem. Lett.* **2013**, 691–697.
90. Choi, C. L.; Li, H.; Olson, A. C. K.; Jain, P. K.; Sivasankar, S.; Alivisatos, A. P. Spatially Indirect Emission in a Luminescent Nanocrystal Molecule. *Nano Lett.* **2011**, *11*, 2358–2362.
91. Saunders, A. E.; Popov, I.; Banin, U. Synthesis of Hybrid CdS–Au Colloidal Nanostructures. *J. Phys. Chem. B* **2006**, *110*, 25421–25429.
92. Zhu, H.; Song, N.; Rodríguez-Córdoba, W.; Lian, T. Wave Function Engineering for Efficient Extraction of up to Nineteen Electrons from One CdSe/CdS Quasi-Type II Quantum Dot. *J. Am. Chem. Soc.* **2012**, *134*, 4250–4257.
93. García-Santamaría, F.; Brovelli, S.; Viswanatha, R.; Hollingsworth, J. A.; Htoon, H.; Crooker, S. A.; Klimov, V. I.

Breakdown of Volume Scaling in Auger Recombination in CdSe/CdS Heteronanocrystals: The Role of the Core–Shell Interface. *Nano Lett.* **2011**, *11*, 687–693.
94. Brovelli, S.; Schaller, R. D.; Crooker, S. A.; García-Santamaría, F.; Chen, Y.; Viswanatha, R.; Hollingsworth, J. A.; Htoon, H.; Klimov, V. I. Nano-engineered Electron–Hole Exchange Interaction Controls Exciton Dynamics in Core–Shell Semiconductor Nanocrystals. *Nat Commun.* **2011**, *2*, 280.
95. Htoon, H.; Malko, A. V.; Bussian, D.; Vela, J.; Chen, Y.; Hollingsworth, J. A.; Klimov, V. I. Highly Emissive Multiexcitons in Steady-State Photoluminescence of Individual "Giant" CdSe/CdS Core/Shell Nanocrystals. *Nano Lett.* **2010**, *10*, 2401–2407.
96. Garcia-Santamaria, F.; Chen, Y. F.; Vela, J.; Schaller, R. D.; Hollingsworth, J. A.; Klimov, V. I. Suppressed Auger Recombination in "Giant" Nanocrystals Boosts Optical Gain Performance. *Nano Lett.* **2009**, *9*, 3482–3488.
97. Reynolds, G. A.; Drexhage, K. H. New Coumarin Dyes with Rigidized Structure for Flashlamp-Pumped Dye Lasers. *Opt. Commun.* **1975**, *13*, 222–225.
98. Kubin, R. F.; Fletcher, A. N. Fluorescence Quantum Yields of Some Rhodamine Dyes. *J. Lumin.* **1982**, *27*, 455–462.
99. Klimov, V. I. Optical Nonlinearities and Ultrafast Carrier Dynamics in Semiconductor Nanocrystals. *J. Phys. Chem. B* **2000**, *104*, 6112–6123.
100. Huang, J. E.; Huang, Z. Q.; Jin, S. Y.; Lian, T. Q. Exciton Dissociation in CdSe Quantum Dots by Hole Transfer to Phenothiazine. *J. Phys. Chem. C* **2008**, *112*, 19734–19738.
101. Huang, J.; Stockwell, D.; Huang, Z. Q.; Mohler, D. L.; Lian, T. Q. Photoinduced Ultrafast Electron Transfer from CdSe Quantum Dots to Re-bipyridyl Complexes. *J. Am. Chem. Soc.* **2008**, *130*, 5632–5633.
102. Jiang, Z.-J.; Kelley, D. F. Hot and Relaxed Electron Transfer from the CdSe Core and Core/Shell Nanorods. *J. Phys. Chem. C* **2011**, *115*, 4594–4602.
103. Srivastava, A.; Htoon, H.; Klimov, V. I.; Kono, J. Direct Observation of Dark Excitons in Individual Carbon Nanotubes: Inhomogeneity in the Exchange Splitting. *Phys. Rev. Lett.* **2008**, *101*, 087402.
104. Klimov, V. I. Spectral and Dynamical Properties of Multiexcitons in Semiconductor Nanocrystals. *Annu. Rev. Phys. Chem.* **2007**, *58*, 635–673.
105. Yang, Y.; Rodríguez-Córdoba, W. E.; Lian, T. Ultrafast Charge Separation and Recombination Dynamics in Lead Sulfide Quantum Dot-Methylene Blue Complexes Probed by Electron and Hole Intraband Transitions. *J. Am. Chem. Soc.* **2011**, *133*, 9246–9249.
106. Chen, O.; Zhao, J.; Chauhan, V. P.; Cui, J.; Wong, C.; Harris, D. K.; Wei, H.; Han, H.-S.; Fukumura, D.; Jain, R. K.; *et al.* Compact High-Quality CdSe–CdS Core–Shell Nanocrystals with Narrow Emission Linewidths and Suppressed Blinking. *Nat. Mater.* **2013**, *12*, 445–451.
107. Burda, C.; Green, T. C.; Link, S.; El-Sayed, M. A. Electron Shuttling across the Interface of CdSe Nanoparticles Monitored by Femtosecond Laser Spectroscopy. *J. Phys. Chem. B* **1999**, *103*, 1783–1788.
108. McArthur, E. A.; Morris-Cohen, A. J.; Knowles, K. E.; Weiss, E. A. Charge Carrier Resolved Relaxation of the First Excitonic State in CdSe Quantum Dots Probed with Near-Infrared Transient Absorption Spectroscopy. *J. Phys. Chem. B* **2010**, *114*, 14514–14520.
109. Zhu, H. M.; Song, N. H.; Lian, T. Q. Controlling Charge Separation and Recombination Rates in CdSe/ZnS Type I Core-Shell Quantum Dots by Shell Thicknesses. *J. Am. Chem. Soc.* **2010**, *132*, 15038–15045.
110. Norris, D. J.; Efros, A. L.; Rosen, M.; Bawendi, M. G. Size Dependence of Exciton Fine Structure in CdSe Quantum Dots. *Phys. Rev. B* **1996**, *53*, 16347–16354.
111. Goss, F. R. 173. The Magnitude of the Solvent Effect in Dipole-Moment Measurements. Part III. Polarisation and Association of Alcohols in the Liquid Phase. *J. Chem. Soc.* **1940**, *0*, 888–894.
112. Loudon, R. One-Dimensional Hydrogen Atom. *Am. J. Phys.* **1959**, *27*, 649–655.
113. Wu, K.; Liu, Z.; Zhu, H.; Lian, T. Exciton Annihilation and Dissociation Dynamics in Group II-V Cd3P2 Quantum Dots. *J. Phys. Chem. A* **2013**, 10.1021/jp402511m.
114. Wu, K.; Song, N.; Liu, Z.; Zhu, H.; Rodríguez-Córdoba, W. E.; Lian, T. Interfacial Charge Separation and Recombination in InP and Quasi-type II InP/CdS Core/Shell Quantum Dot-Molecular Acceptor Complexes. *J. Phys. Chem. A* **2013**, 10.1021/jp402425w.